Improving Microwave Imaging by Enhancing Diffraction Tomography

R. D. Murch, *Member, IEEE*, and T. K. K. Chan

Abstract— **In this paper, a technique for enhancing the reconstruction quality of diffraction tomography for microwave imaging is presented. The technique invokes the WKB approximation in conjunction with utilizing measurement data at more than one frequency to overcome some of the limitations of diffraction tomography. The resulting formulation has a mathematical interpretation which leads to some interesting insights into the limitations of diffraction tomography. Numerical implementation of the technique is also described and actual simulation results using this implementation for a variety of two-dimensional (2-D) objects are provided. These show that indeed significant improvements over conventional diffraction tomography are possible with our enhanced technique.**

I. Introduction

MICROWAVE imaging has potentially many important technological applications. These include medical imaging [1], nondestructive testing [2], geophysics [3], and robotic vision [2]. The advantages microwave imaging offers over more conventional imaging techniques are numerous. They include the relatively low health hazard of nonionizing low power microwaves, its ability to image properties such as permittivity and conductivity, and the likely cost competitiveness of the imaging equipment. Consequently microwave imaging has attracted much interest from researchers in recent times [1]–[9].

The difficulty with microwave imaging, however, is the associated problem with performing object reconstruction. Because microwaves experience significant attenuation, scattering, and diffraction standard tomographic reconstruction schemes are not readily applicable and are of only limited usefulness. In an attempt to overcome this problem, two approaches to microwave imaging have been investigated in the recent past [10]. The first is based on diffraction tomography under either the Born or Rytov approximations. The advantage of this approach is that it is comparatively straightforward to apply and usually computationally efficient. The disadvantage, however, is that due to the underlying approximations involved the type of objects imaged accurately are usually limited [4]. The second approach utilizes some form of exact description of wave motion to formulate reconstruction as a nonlinear equation which is solved numerically. The advantage is that in principle any object type can be imaged accurately since wave motion is described exactly [11]. However, in practice the computational overheads of this approach are usually so large that restrictions on either the object size or type of object must be enforced [11].

In this paper, an attempt to fill the middle ground between these approaches is performed. We describe a method that utilizes the comparatively straightforward formulation of diffraction tomography while incorporating some of the more intricate wave phenomena found in the approaches based on exact descriptions of the underlying wave motion. The inspiration for our technique is that it invokes concepts from the WKB high frequency approximation in conjunction with utilizing scattering measurements at more than one frequency. Not only do the simulation results reveal that significant improvements are possible in image quality, but the resulting interpretation of diffraction tomography by our method also illuminates some interesting new concepts.

Alternative solutions have been devised in an attempt to overcome limitations associated with diffraction tomography. However, these methods either require *a priori* information about the object [12], [13], or when no *a priori* information is required, the few numerical results so far presented do not suggest that the improvements are likely to be spectacular [14]–[16].

In Section II, necessary preliminaries are introduced to define our microwave imaging problem. The theory of our enhancements to diffraction tomography are formally introduced in Section III where the interpretation of our formulation is given. The methods for implementing and reconstructing objects under our solution are then given in Section IV. Simulation results are presented in Section V and these results are compared to what are obtained when the conventional Born approximation is invoked. Finally, in Section VI and Section VII discussions and conclusions are given to examine the validity and significance of our technique.

II. Preliminaries

Arbitrarily chosen (but considered fixed, once chosen) Cartesian coordinates x, y, and z are set up in three-dimensional (3-D) space. Scattering objects with cylindrical symmetry in the z-direction are considered so that our objects can be considered two-dimensional (2-D) with only variations in the 2-D xy-plane. We denote the 2-D xy-plane by Υ and partition it as $\Upsilon = \Upsilon_+ \cup \Upsilon_-$ so that Υ_- represents the region of 2-D space in which the scattering object exists. The scattering object is assumed to have permittivity $\epsilon(x, y)$ and permeability μ_0 and to be surrounded by free space (ϵ_0, μ_0).

Manuscript received September 13, 1995; revised November 27, 1995. This work was supported by Grant HKUST 198/93E from the Hong Kong University Grants Committee

The authors are with the Department of Electrical and Electronic Engineering, Hong Kong University of Science and Technology, Clear Water Bay, Kowloon, Hong Kong.

Publisher Item Identifier S 0018-9480(96)01542-6

We consider electromagnetic wave motion polarized in the z-direction with free-space angular frequency ω. The electromagnetic wave motion can then be uniquely described by the z-component of the electric field E_z [17]. We write E_z as a function of (2-D) space Υ and the free-space wavenumber $k = \omega\sqrt{\epsilon_0\mu_0}$ and suppress a time dependence of $e^{j\omega t}$. E_z then satisfies

$$(\nabla^2 + k^2)E_z(\mathbf{x}, k) = -k^2 V E_z(\mathbf{x}, k) \tag{1}$$

where $\nabla^2 = \partial_x^2 + \partial_y^2$ and the scattering potential V is related to the permittivity and, hence, the refractive index $n(x, y)$ by

$$\begin{aligned} V(x, y) &= \frac{\epsilon(x, y)}{\epsilon_0} - 1 \\ &= n^2(x, y) - 1 \end{aligned} \tag{2}$$

and is assumed to be nonzero only in the region Υ_-.

We also find it desirable to partition E_z into its incident, $E_z^i(\mathbf{x}, k)$, and scattered, $E_z^s(\mathbf{x}, k)$, components so that $E_z(\mathbf{x}, k) = E_z^i(\mathbf{x}, k) + E_z^s(\mathbf{x}, k)$. We take the incident wavefield to be planar and write it as

$$E_z^i(\mathbf{x}, k) = e^{-jk\hat{\mathbf{k}}\,\mathbf{x}} \tag{3}$$

where $\hat{}$ implies a unit vector and $\mathbf{k}$ is the direction of propagation. We take as our scattering data, measurements of $E_z^s(\mathbf{x}, k)$ in the far field which we denote as $E_z^{ffs}(\hat{\mathbf{x}}, k\hat{\mathbf{k}})$ and define by

$$E_z^s(\hat{\mathbf{x}}, k) = E_z^{ffs}(\hat{\mathbf{x}}, k\hat{\mathbf{k}})\frac{e^{-jk|\mathbf{x}|}}{\sqrt{8\pi k|\mathbf{x}|}}. \tag{4}$$

We include the vector $\hat{\mathbf{k}}$ in the argument of $E_z^{ffs}(\hat{\mathbf{x}}, k\hat{\mathbf{k}})$ to indicate that the incident field (3) with propagation direction $\mathbf{k}$ was invoked to generate it.

The essence of our microwave imaging problem can now be simply stated. We wish to estimate the refractive index distribution $n(\mathbf{x})$ within Υ_- from measurements of the far field $E_z^{ffs}(\mathbf{x}, k\hat{\mathbf{k}})$. We perform this by developing enhancements to diffraction tomography.

III. Enhancing Diffraction Tomography

Our enhancement to diffraction tomography can be obtained by appealing to the derivation invoked for the Born approximation. Consequently, we begin by considering the expression for $E_z^s(\mathbf{x}, k)$ in the far field. By invoking the far-field form of the Green's function [17, p. 611]

$$g(\mathbf{x}, \mathbf{x}_1) = \frac{e^{-jk(|\mathbf{x}| - \mathbf{x}_1\,\hat{\mathbf{x}})}}{\sqrt{8\pi k|\mathbf{x}|}} \tag{5}$$

the far field can be written as

$$\begin{aligned} E_z^{ffs}(\hat{\mathbf{x}}, k\hat{\mathbf{k}}) = \int_{\Upsilon_-} & k^2\,[n^2(\mathbf{x}_1) - 1]E_z(\mathbf{x}_1, k) \\ & \cdot e^{jk\mathbf{x}\cdot\mathbf{x}_1}\,d\Upsilon(\mathbf{x}_1) \end{aligned} \tag{6}$$

where integration is with respect to $\mathbf{x}_1$ over the region Υ_-. By now multiplying and dividing the integrand of (6) by the planar incident field (3) this equation can be manipulated into the form

$$\begin{aligned} E_z^{ffs}(\hat{\mathbf{x}}, k\hat{\mathbf{k}}) = \int_{\Upsilon_-} & k^2\,[n^2(\mathbf{x}_1) - 1]E_z(\mathbf{x}_1, k) \\ & \cdot e^{jk\mathbf{k}\,\mathbf{x}_1}e^{-jk\mathbf{k}\,\mathbf{x}_1}e^{jk\mathbf{x}\,\mathbf{x}_1}\,d\Upsilon(\mathbf{x}_1) \end{aligned} \tag{7}$$

which can be further rewritten as

$$\begin{aligned} E_z^{ffs}(\hat{\mathbf{x}}, k\hat{\mathbf{k}}) = \int_{\Upsilon_-} & k^2\,[n^2(\mathbf{x}_1) - 1]D(\mathbf{x}_1, k\hat{\mathbf{k}}) \\ & \cdot e^{-jk(\mathbf{k}-\mathbf{x})\,\mathbf{x}_1}\,d\Upsilon(\mathbf{x}_1) \end{aligned} \tag{8}$$

where

$$D(\mathbf{x}, k, \hat{\mathbf{k}}) = E_z(\mathbf{x}, k)e^{jk\hat{\mathbf{k}}\,\mathbf{x}} \tag{9}$$

We here term $D(\mathbf{x}, k, \hat{\mathbf{k}})$ as the distortion function. For situations in which the Born approximation is valid, the distortion function is approximately unity for all incident directions and so (8) can be written as a Fourier transform and the standard results of diffraction tomography will apply [10]. That is

$$E_z^{ffs}(\mathbf{x}, k\hat{\mathbf{k}}) = k^2\mathcal{F}_2\{[n^2(\mathbf{x}_1) - 1]\}(\mathbf{k}') \tag{10}$$

where $\mathbf{k}' = k(\hat{\mathbf{k}} - \hat{\mathbf{x}})$ and the 2-D Fourier transform $\mathcal{F}_2$ is defined by

$$\mathcal{F}_2[f(\mathbf{x})](\mathbf{u}) = \int_{-\infty}^{\infty}\int_{-\infty}^{\infty} f(\mathbf{x})e^{-j\mathbf{u}\,\mathbf{x}}\,d\mathbf{x}. \tag{11}$$

However, when the distortion function cannot be approximated by unity then the Born approximation will not be valid and the resulting reconstruction will not be accurate. In this situation, the distortion function can be thought of as accounting for the difference between the planar incident field and the actual field in Υ_-. Consequently, in order to improve upon the Born approximation it is necessary to try and remove the effect of the distortion function. The difficulty with this, however, is that the distortion function is different for each $\hat{\mathbf{k}}$ and k preventing a straightforward Fourier relationship to be written as for the Born approximation. Here, our approach to overcome this is to first approximately estimate the distortion function for each $\hat{\mathbf{k}}$ and k and then later remove its effect.

To proceed with this approach at enhancing the Born approximation it is useful to define the following Fourier transforms with respect to $\mathbf{x}$

$$\tilde{O}(\mathbf{u}) = k^2\mathcal{F}_2\{[n^2(\mathbf{x}) - 1]\}(\mathbf{u}) \tag{12}$$

$$\tilde{D}_{\mathbf{k}}(\mathbf{u}) = \mathcal{F}_2[D(\mathbf{x}, k, \hat{\mathbf{k}})](\mathbf{u}). \tag{13}$$

The subscript $\mathbf{k}$ has been included to stress that the transform pairs are with respect to $\mathbf{x}$ only and all other variables have been taken to be independent so that $\tilde{D}_{\mathbf{k}}(\mathbf{u})$ is a 2-D function of $\mathbf{u}$ which is different for each $\mathbf{k}$.

By now taking the convolution of the terms in (12) and (13) we get

$$\tilde{F}_{\mathbf{k}}(\mathbf{u}) = \tilde{O}(\mathbf{u}) \circledcirc \tilde{D}_{\mathbf{k}}(\mathbf{u}) \tag{14}$$

where $\circledcirc$ is used to denote convolution. By making comparisons with (8) and realizing that convolution in the Fourier

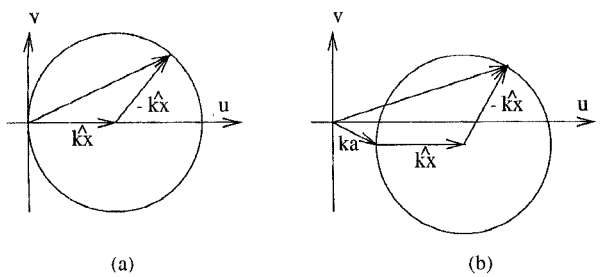

(a) (b)

Fig. 1. Locus in Fourier space corresponding to the observable spectrum $\tilde{O}(\mathbf{u})$ of the object for (a) the conventional Born approximation and (b) the enhanced approximation (24).

domain becomes multiplication in the object domain it can be deduced that for fixed $\hat{\mathbf{k}}$ equations (8) and (14) are equivalent when $\mathbf{u} = k(\hat{\mathbf{k}} - \hat{\mathbf{x}})$. That is

$$E_z^{ffs}(\hat{\mathbf{x}}, k\hat{\mathbf{k}}) = \tilde{F}_{\hat{\mathbf{k}}}(\mathbf{u}) \quad \text{when} \quad \mathbf{u} = k(\hat{\mathbf{k}} - \hat{\mathbf{x}}). \tag{15}$$

Hence, we can only observe $\tilde{F}_{\hat{\mathbf{k}}}(\mathbf{u})$ for points on the locus $\mathbf{u} = k(\hat{\mathbf{k}} - \hat{\mathbf{x}})$. This illustrates the difficulty of our problem since if we knew $\tilde{F}_{\hat{\mathbf{k}}}(\mathbf{u})$ for all $\mathbf{u}$ then we could use a blind deconvolution algorithm to estimate the distortion function and remove its effect and, hence, recover the object $\tilde{O}(\mathbf{u})$. However, because we can only observe $\tilde{F}_{\hat{\mathbf{k}}}(\mathbf{u})$ on a finite locus of points we must invoke another means of estimating the distortion function.

Estimating the distortion function can be achieved by understanding it further. This is achieved by representing $E_z(\mathbf{x}, k)$ as a WKB high frequency approximation [17]. The distortion function then becomes

$$D(\mathbf{x}, k, \hat{\mathbf{k}}) = e^{-jk[S(\mathbf{x}) - \hat{\mathbf{k}}\,\mathbf{x}]} \tag{16}$$

where we have invoked the WKB approximation $E_z(\mathbf{x}, k) = e^{-jkS(\mathbf{x})}$ in which $S(\mathbf{x})$ denotes the wavefronts of the field which depend on $\hat{\mathbf{k}}$. So now the problem of estimating the distortion function has been reduced to estimating the wavefronts $S(\mathbf{x})$.

To simplify matters we choose to represent the difference $[S(\mathbf{x}) - \hat{\mathbf{k}} \cdot \mathbf{x}]$ in (16) as a 2-D Taylor series expansion about the origin so that

$$S(\mathbf{x}) - \hat{\mathbf{k}} \cdot \mathbf{x}_1 = a_{00} + (a_{10}x + a_{01}y) + \frac{1}{2!}(x^2 a_{20} + 2xya_{11} + a_{02}y^2) + \cdots \tag{17}$$

where the constants a_{mn}, for $m, n \in \{0, 1, \cdots, \}$ represent the partial derivatives of $[S(\mathbf{x}) - \hat{\mathbf{k}} \cdot \mathbf{x}]$ about the origin with the m and n, respectively, referring to the number of derivatives with respect to x and y. It should also be noted that the a_{mn} are functions of $\hat{\mathbf{k}}$. When the Born approximation is valid the difference $[S(\mathbf{x}) - \hat{\mathbf{k}} \cdot \mathbf{x}]$ will be small and, hence, the coefficients will also be all small. However, when the Born approximation is not valid and the coefficients are large some means of estimating them is required so their effect can be removed.

By substituting (17) into (16) and invoking some well known Fourier transform pairs [18] we can then write the Fourier transform (12) of the distortion function as

$$\tilde{D}_{\hat{\mathbf{k}}}(\mathbf{u}) = e^{jka_{00}}\delta(u + ka_{10}, v + ka_{01}) \odot \left\{\exp\left[j\left(\frac{u^2}{b_{20}} + \frac{uv}{2b_{11}} + \frac{v^2}{b_{02}}\right)\right]\right\} \odot \mathcal{F}_2[e^{(\cdot)}](\mathbf{u}) \tag{18}$$

where the 2-D delta function is denoted by $\delta(\cdot, \cdot)$ and the exact relation of the coefficients b_{20}, b_{11}, and b_{02} to the a_{20}, a_{11}, and a_{02} is not important here and not listed.

We can then substitute (18) into (14) to obtain

$$\tilde{F}_{\hat{\mathbf{k}}}(\mathbf{u}) = \tilde{O}(\mathbf{u}) \odot [e^{jka_{00}}\delta(u + ka_{10}, v + ka_{01})] \odot \left\{\exp\left[j\left(\frac{u^2}{b_{20}} + \frac{uv}{2b_{11}} + \frac{v^2}{b_{02}}\right)\right]\right\} \odot \mathcal{F}_2[e^{(\cdots)}](\mathbf{u}) \tag{19}$$

where it should be noted again that $E_z^{ffs}(\hat{\mathbf{x}}, k\hat{\mathbf{k}}) = \tilde{F}_{\hat{\mathbf{k}}}(\mathbf{u})$ when $\mathbf{u} = k(\hat{\mathbf{k}} - \hat{\mathbf{x}})$ and that the a_{mn} will be different for each $\hat{\mathbf{k}}$.

The expression (19) forms the essence of our improvements to the Born approximation. Its significance can be best understood by considering its effect on the observable (observable from $E_z^{ffs}(\hat{\mathbf{x}}, k\hat{\mathbf{k}})$) part of the spectrum of $\tilde{O}(\mathbf{u})$ and by making comparisons with the conventional Born approximation. For the Born approximation the observable part of the spectrum of $\tilde{O}(\mathbf{u})$ corresponds to the locus of points described by the extremity of the vector $\mathbf{u} = k(\hat{\mathbf{k}} - \hat{\mathbf{x}})$ and is a circle centered at $k\hat{\mathbf{k}}$ and whose radius is k [4]. This is illustrated in Fig. 1(a). When we take into account the distortion function, the observable part of the spectrum of $\tilde{O}(\mathbf{u})$ is somewhat altered. To understand how it is altered it is useful to consider the effects of the individual a_{mn} in turn. The first coefficient a_{00} simply adds an additional phase term $e^{jka_{00}}$ to the spectrum. The second set of terms in our expansion (those corresponding to a_{10} and a_{01} in the delta function) translate the observable part the spectrum of $\tilde{O}(\mathbf{u})$ by ka_{10} and ka_{01} in the u and v coordinate directions, respectively, [by $-ka_{10}$ and $-ka_{01}$ with respect to the origin of $\tilde{F}_{\hat{\mathbf{k}}}(\mathbf{u})$]. If we let $\mathbf{a} = (a_{10}, a_{01})^T$ then the corresponding locus of points is described by the extremity of the vector $\mathbf{u} = k(\hat{\mathbf{k}} + \mathbf{a} - \hat{\mathbf{x}})$ and is a circle centered at $k(\hat{\mathbf{k}} + \mathbf{a})$ whose radius is k. This is illustrated in Fig. 1(b). The effect of the distortion function can clearly be seen as a translation of the observable part of the spectrum which will be different for each $\hat{\mathbf{k}}$. The third set of terms in our expansion distorts the value of the spectrum on the locus by a convolution with a Gaussian-like function. If the coefficients are small, then the Gaussian will be narrow, causing minor distortion. The remaining higher order terms in the series will also cause distortion; however, we will not consider their detailed effects further other than to say they will be small if their corresponding coefficients are also small. It can also be seen that the Born approximation is a special example of (19) when all the coefficients a_{mn} are taken to be zero and, hence, there is no translation or phase shift.

Clearly, if we could estimate some of the a_{mn} from the measurement data then we could correct for the distortion connected with the additional phase and translations. In this

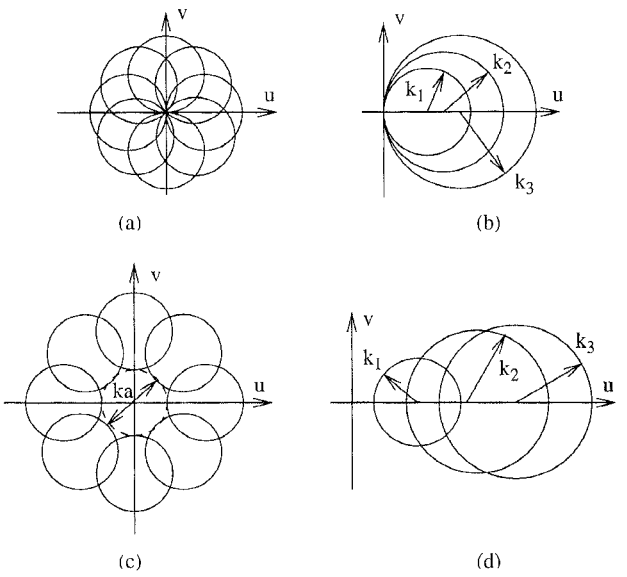

Fig 2. Area corresponding to the observable part of the spectrum $\tilde{O}(\mathbf{u})$ of the object under the conventional and enhanced Born approximations when either k or $\hat{\mathbf{k}}$ are varied. For the conventional Born approximation, the coverage of the spectrum is as (a) when $\hat{\mathbf{k}}$ is varied for fixed k and is as (b) when k is varied for fixed $\hat{\mathbf{k}}$. For the enhanced Born approximation the coverage of the spectrum is as (c) when $\hat{\mathbf{k}}$ is varied for fixed k and is as (d) when k is varied for fixed $\hat{\mathbf{k}}$. The effect of the translation is clearly visible for the enhanced approximation

way, we could provide enhancements to the Born approximation and, hence, diffraction tomography. Before proceeding with attempting to estimate the a_{mn}, which is discussed in the next section, it is useful to discuss two further aspects of the interpretation of the distortion function.

The first result concerns how the spectrum of $\tilde{O}(\mathbf{u})$ can be collected over 2-D space so a 2-D inverse Fourier transform can be invoked to reconstruct the object $O(\mathbf{u})$ and, hence, the refractive index $n(\mathbf{x})$. Under the conventional Born approximation this is generally performed by collecting measurements over a range of propagation directions $\hat{\mathbf{k}}$, so that the locus in Fig. 1(a) is rotated about the origin. The result is shown in Fig. 2(a). An alternative method sometimes used is to utilize a range of k but fixed $\hat{\mathbf{k}}$. The coverage thereby achieved is shown in Fig. 2(b). However, under our interpretation of the distortion function this conventional interpretation is somewhat altered. The result of incorporating the effect of the distortion function for the two situations just described are given in Fig. 2(c) and (d). It should be clear the translation caused by the distortion function has a significant effect on the coverage achieved and is different from the conventional interpretation.

The second result worth discussing is deducing the approximate physical meaning of the coefficients a_{mn}. These depend on the wavefronts $S(\mathbf{x})$ and so to gain insight, we approximate the wavefronts by assuming that they do not refract significantly and travel along the same path as the incident wavefield. The electrical path length of the wavefronts is then simply the integral of the refractive index along straight paths. For planar incident waves propagating along the x-axis $S(\mathbf{x})$ can then be approximately written as

$$S(x_0, y) \approx \int_{-\infty}^{x_0} n(x, y)\, dx. \tag{20}$$

The coefficients can then be estimated by taking the derivatives of the difference (17). For example if the object is a circular cylinder with radius r_0 and center at the origin then a_{00} can be approximated by

$$a_{00} \approx r_0[n(0, 0) - 1]. \tag{21}$$

The coefficients a_{10} and a_{01} have a similar physical meaning based on (20). By taking derivatives at the origin we can also approximately define a_{10} and a_{01} as

$$a_{10} \approx [n(0, 0) - 1]$$

and

$$a_{01} \approx 0. \tag{22}$$

Thus it is clear the coefficients depend intimately on the object. However, in our imaging problem we must estimate the unapproximated coefficients from the measurement data alone.

IV. Estimating the Distortion Function

To alleviate the estimation process, we introduce various levels of enhancements by considering only a limited number of terms in the Taylor series (17). In particular we introduce three levels of enhancements and these are written as

$$\tilde{F}(\mathbf{u}) = \tilde{O}(\mathbf{u}) e^{jka_{00}} \tag{23}$$

$$\tilde{F}(\mathbf{u}) = \tilde{O}(\mathbf{u}) \odot [e^{jka_{00}} \delta(u + ka_{10}, v + ka_{01})] \tag{24}$$

$$\tilde{F}(\mathbf{u}) = \tilde{O}(\mathbf{u}) \odot [e^{jka_{00}} \delta(u + ka_{10}, v + ka_{01})] \odot \left\{ \exp\left[j \left(\frac{u^2}{b_{20}} + \frac{uv}{2b_{11}} + \frac{v^2}{b_{02}} \right) \right] \right\} \tag{25}$$

where it should be noted again that $E_z^{ffs}(\hat{\mathbf{x}}, k\hat{\mathbf{k}}) = \tilde{F}_{\hat{\mathbf{k}}}(\mathbf{u})$ when $\mathbf{u} = k(\hat{\mathbf{k}} - \hat{\mathbf{x}})$ and that the a_{mn} will be different for each $\hat{\mathbf{k}}$. Clearly, each of the equations takes into account an additional term in the distortion function. We refer to the various levels of enhancement represented by (23)–(25) as, respectively, enhancements one, two, and three. In Sections IV-A–IV-C we describe methods for estimating the terms in the distortion function for each of the enhancements.

A. Estimation for Enhancement One

Enhancement one is written in (23). Mathematically, it corresponds to when only the a_{00} term is assumed significant and the remaining a_{mn} assumed negligible. Consequently, only a_{00} need be estimated.

The technique adopted here for estimating a_{00} is based upon calculating $E_z^{ffs}(\hat{\mathbf{x}}, k\hat{\mathbf{k}})$ for two wavenumbers, k_1 and k_2, say. From our earlier discussion, we know that this gives us spectral information about $e^{jka_{00}}[n^2(\mathbf{x}) - 1]$ on two circles of radius k_1 and k_2. Because we are also assuming that only a_{00} is significant, we know these two circles intersect at the origin of Fourier space since a_{10} and a_{01} are taken as zero. The point of intersection occurs when $\hat{\mathbf{x}} = \hat{\mathbf{k}}$, the forward-scattering

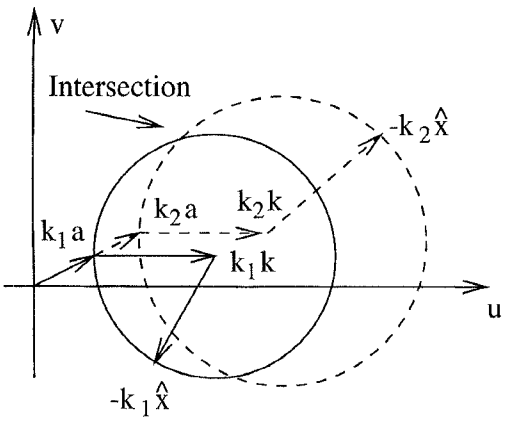

Fig. 3. Illustration of our technique for estimating a_{10} and a_{01} for the enhanced Born approximation.

direction. We also know at this point of intersection that the value of the far field at k_1 and k_2 differs from the spectrum of $\tilde{O}(\mathbf{u})$ by, respectively, the phase factors $e^{jk_1a_{00}}$ and $e^{jk_2a_{00}}$. A straightforward estimate of a_{00} can consequently be obtained from the difference between the phases of $E_z^{ffs}(\hat{\mathbf{x}}, k_1\hat{\mathbf{k}})$ and $E_z^{ffs}(\hat{\mathbf{x}}, k_2\hat{\mathbf{k}})$ in the forward direction $\hat{\mathbf{x}} = \hat{\mathbf{k}}$. This may be expressed as

$$a_{00} = \frac{\angle E_z^{ffs}(\hat{\mathbf{x}}, k_2\hat{\mathbf{k}}) - \angle E_z^{ffs}(\hat{\mathbf{x}}, k_1\hat{\mathbf{k}})}{k_2 - k_1} \tag{26}$$

where $\hat{\mathbf{x}}$ is taken in the forward direction $\hat{\mathbf{k}}$, and $\angle$ denotes the phase of.

Although this process is reasonably straightforward, reconstruction by simply altering the phase will likely produce improvements to the Born approximation.

B. Estimation for Enhancement Two

Enhancement two is written in (24). It takes into account an additional term in the distorting function as compared to enhancement one. Consequently, a_{00}, a_{10}, and a_{01} need to be estimated.

The technique adopted for estimating the coefficients is to again calculate $E_z^{ffs}(\hat{\mathbf{x}}, k\hat{\mathbf{k}})$ for two wavenumbers, k_1 and k_2 say. This case, however, gives us spectral information about $e^{jka_{00}}\tilde{O}(\mathbf{u})$ on two circles of radius k_1 and k_2, which not only have different diameters but are also translated by the coefficients a_{10} and a_{01}, as shown in Fig. 3. This implies that the intersection point of the circles is now shifted away from the origin. At this intersection point the value of $E_z^{ffs}(\mathbf{x}, k\hat{\mathbf{k}})/k^2$ for k_1 and k_2 will equate apart from the phase factors $e^{jk_1a_{00}}$ and $e^{jk_2a_{00}}$.

Consequently, a straightforward method to estimate the translation introduced by a_{01} and a_{10} is to find a point where $|E_z^{ffs}(\mathbf{x}, k_1\hat{\mathbf{k}})/k_1^2|$ and $|E_z^{ffs}(\mathbf{x}, k_2\hat{\mathbf{k}})/k_2^2|$ equate. At this point we can then use (26) to determine a_{00}. Clearly, in practice there might be several points where the field values equate so to eliminate this possibility we invoke measurements from more than just two values of k (usually we utilize five different k).

To formalize this procedure we write a cost function as

$$C(a_{00}, a_{10}, a_{01}) = \sum_{p \neq q} \| e^{jk_pa_{00}} E_{ffs}(\hat{\mathbf{x}}, k_p\hat{\mathbf{k}})/k_p^2 - e^{jk_qa_{00}} E_{ffs}(\hat{\mathbf{x}}, k_q\hat{\mathbf{k}})/k_q^2 \| \tag{27}$$

where p and q run over the number of measurements taken and $\hat{\mathbf{x}}$ is taken at the point of intersection. We then determine the a_{10} and a_{01} that minimizes this cost function. A straightforward method for finding the minimum is to invoke an exhaustive search. The computational intensive nature of this can be reduced by realizing that the vector made up as $(a_{10}, a_{01})^T$ will approximately point in the direction of $\hat{\mathbf{k}}$ and so we can restrict our search area appropriately. The search procedure essentially takes three steps and these are: 1) choose a particular a_{10} and a_{01} and find the corresponding intersection points; 2) calculate a_{00} at this intersection point by utilizing (26) and calculate (27); and 3) choose the next a_{10} and a_{01} and repeat the above steps until a global minimum of the cost function is found.

C. Estimation for Enhancement Three

Estimating the third and further terms in the series is in principle different from determining the first and second terms. This is because the third and further terms in the distortion function have effects over a finite area in the Fourier domain. Consequently, to estimate them one needs to know the spectrum also over a finite area. However, because the measurement data only allows us to observe the spectrum on a locus of points described by a circle this is difficult. Consequently, we have been unable to suggest a practical method for performing this. A possible avenue, however, would be to utilize a continuum of k and try and estimate the effects of the third term from these.

V. Simulation Results

In this section, simulation results of reconstructing or imaging objects under enhancement one and two are described so that the performance and significance of the enhancements can be demonstrated.

A necessary part of simulating reconstruction algorithms is obtaining suitable measurement data upon which the reconstruction algorithm will operate. In general, this is nontrivial and so we restrict our objects to various configurations of concentric and nonoverlapping eccentric cylinders in which each cylinder has an arbitrary constant refractive index which is real and nonnegative. The measurement data from these objects is calculated by the exact formulation of mode-matching and addition theorems (to effect mode-matching on eccentric cylinders) [17]. The data so obtained is completely independent of the inversion method and consequently, will form an unbiased test for our enhancements. To make some quantitative comments about our simulations, we also find it useful to define L to be the largest linear dimension, in wavelengths, of the particular object under consideration.

In the simulations of enhancement one, we utilize measurements from two wavenumbers whose ratio is $k_1/k_2 = 1.1$.

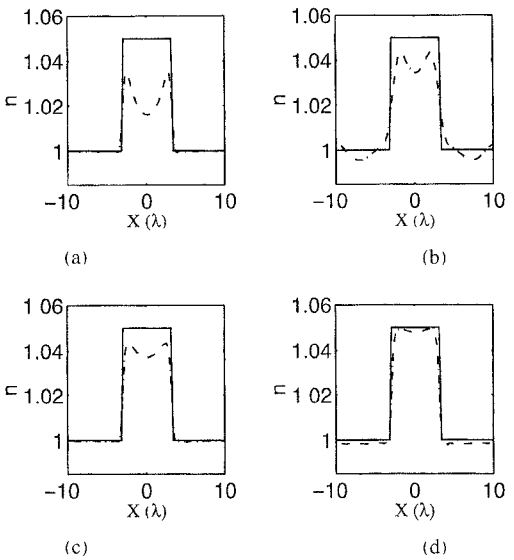

Fig. 4. Simulation results of reconstruction of an object consisting of a single cylinder of radius $r_1 = 3\lambda$ and refractive index $n_1 = 1.05$. The results are for (a) Born approximation, (b) Rytov approximation, (c) enhancement one, and (d) enhancement two. The solid and broken lines, respectively, represent the original and reconstructed object profiles

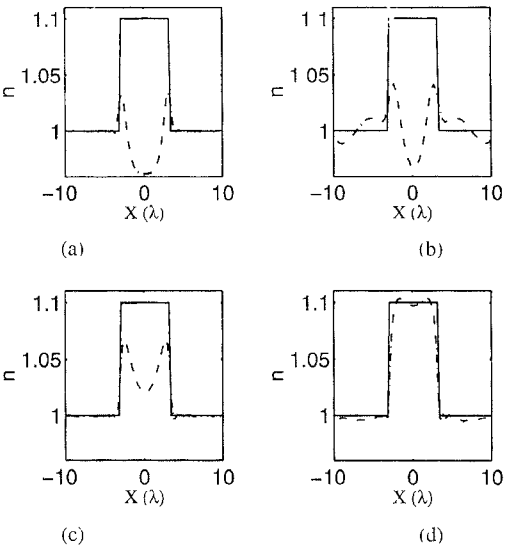

Fig. 5 Simulation results of reconstruction of an object consisting of a single cylinder of radius $r_1 = 3\lambda$ and refractive index $n_1 = 1.10$ The results are for (a) Born approximation, (b) Rytov approximation, (c) enhancement one, and (d) enhancement two The solid and broken lines, respectively, represent the original and reconstructed object profiles

The value of this ratio has an effect on the noise sensitivity of the reconstruction as discussed at the end of Section V-A.

In the simulations for enhancement two, we use measurements from five wavenumbers, to estimate the coefficients a_{00}, a_{10}, and a_{01}, such that the ratio of the maximum to minimum wavenumber is about five; however, we only use the measurement data from the largest wavenumber for the reconstruction itself. Another important consideration under enhancement two is the effect of data missing at the center of Fourier space as shown in Fig. 2(c). In general, the result of this hole creates a dc offset occurring in the reconstruction. This artifact is annoying in the reconstruction so is best removed. It can be removed by interpolating over the missing low frequency area or by utilizing measurement data from the lowest wavenumber for filling in the missing data in the "hole."

After extracting the various coefficients reconstruction was then performed by backpropagation [19].

A. Circularly Symmetric Objects

The first set of reconstruction results are for circularly symmetric objects which in our case consist of either single cylinders or concentric cylinders. For circularly symmetric objects, the coefficients a_{mn} are the same for all $\hat{\mathbf{k}}$.

Altogether we provide five numerical examples of reconstructions for circular symmetric objects. For each simulation four results are provided and these are reconstruction by: a) the conventional Born approximation as defined in (8) when $D(\mathbf{x}, k, \hat{\mathbf{k}}) = 1$; b) the Rytov approximation using the implementation given in [4]; c) enhancement one as specified in (23); and d) enhancement two as specified in (24). Only the vertical cross section along the x-axis of the cylindrical objects with units of wavelength are illustrated to provide easier comparisons between various results. However, it must not be forgotten that they are in fact circular objects. The first two examples are single cylinders while the other examples consist of concentric cylinders of various refractive indices.

The results of reconstructing the refractive index $n(\mathbf{x})$ for the two single cylinder objects are shown in Figs. 4 and 5. In each figure it can be observed that both of our enhancements perform better than the conventional Born and Rytov approximations and it is only in Fig. 4 for which the conventional Born and Rytov approximations perform reasonably. For the Rytov approximation we should also note that distortion occurs outside the object areas in both these examples. It can also be observed that enhancement two performs the best overall.

The remaining three circular symmetric objects consist of several concentric cylinders of various refractive index. The results are shown in Figs. 6–8. The conventional Born and Rytov approximations perform poorly in all these examples. Again, however, our enhancements perform well and enhancement two performs the best. It should be noted that the example in Fig. 8 has been proposed by other researchers [20] as a canonical object for which inverse algorithms can be compared. Both our enhancements are a significant improvement over the conventional Born and Rytov approximations for this example which is a good result in itself.

To better understand our enhancements we have also tabulated the estimated values for a_{00}, a_{10} and a_{01} in Table I. Alongside these values, we have also listed the values obtained by utilizing our approximate formulation as given in (20)–(22). In the examples, enhancement two agrees well with our approximate values.

Results of reconstruction with added noise contamination are listed in Table II. In our simulations, the contamination was modeled as being additive. The level of the contamination

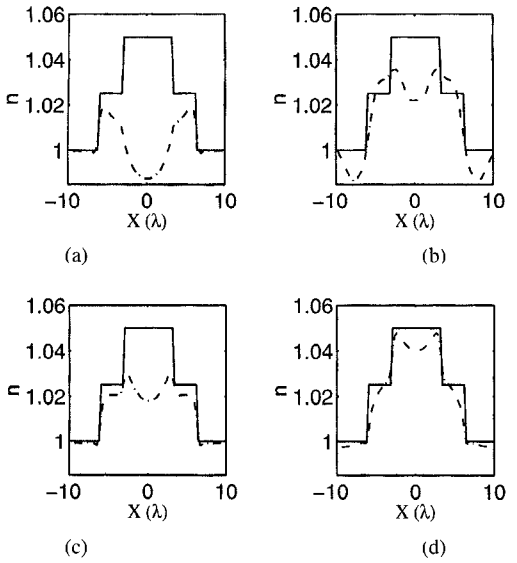

Fig. 6. Simulation results of reconstruction of an object consisting of concentric cylinders with radii $r_1 = 3\lambda$, $r_2 = 6\lambda$, and refractive indices $n_1 = 1.05$, $n_2 = 1.025$, respectively. The results are for (a) Born approximation, (b) Rytov approximation, (c) enhancement one, and (d) enhancement two. The solid and broken lines, respectively, represent the original and reconstructed object profiles.

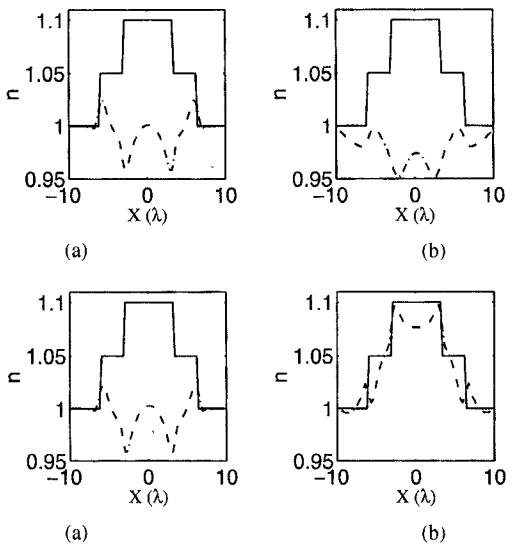

Fig. 7. Simulation results of reconstruction of an object consisting of concentric cylinders with radii $r_1 = 3\lambda$, $r_2 = 6\lambda$ and refractive indices $n_1 = 1.1$, $n_2 = 1.05$, respectively. The results are for (a) Born approximation, (b) Rytov approximation, (c) enhancement one, and (d) enhancement two. The solid and broken lines, respectively, represent the original and reconstructed object profiles.

is specified in decibels (dB) by

$$\mathrm{SNR} = 10 \log_{10} \frac{\overline{c^2}(\mathbf{x})}{\overline{E_z^{ffs^2}}(\mathbf{x})} \tag{28}$$

where the bar and 2 superscript indicate signal power. In our case the data is complex so $c(\mathbf{x})$ is also complex, having both a random magnitude (uniformly distributed in the range 0 to b, where b is a positive constant) and a random phase uniformly distributed in the range $-\pi$ to π. The normalized mean square error (NMSE) between the original reconstruction

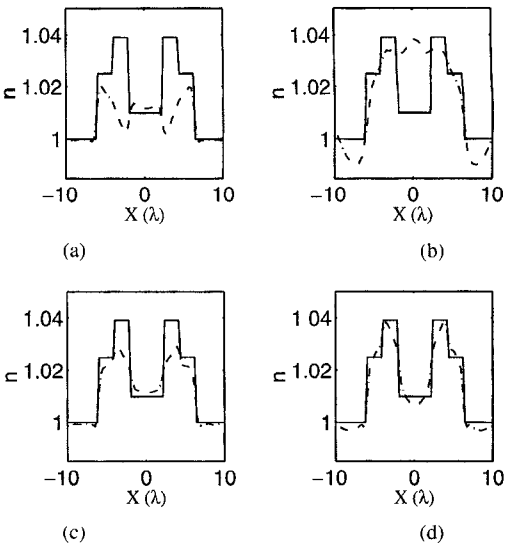

Fig. 8. Simulation results of reconstruction of an object consisting of concentric cylinders with radii $r_1 = 2\lambda$, $r_2 = 4\lambda$, $r_3 = 6\lambda$, and refractive indices $n_1 = 1.010$, $n_2 = 1.039$, $n_3 = 1.025$, respectively (see [20]). The results are for (a) Born approximation, (b) Rytov approximation, (c) enhancement one, and (d) enhancement two. The solid and broken lines, respectively, represent the original and reconstructed object profiles.

$n(\mathbf{x})$ without noise and the degraded reconstruction $\bar{n}(\mathbf{x})$ with noise is defined by

$$NMSE[n(\mathbf{x}), \bar{n}(\mathbf{x})] = 100 \times \frac{\mathrm{Var}\,[n(\mathbf{x}) - \bar{n}(\mathbf{x})]}{\mathrm{Var}\,[n(\mathbf{x})]} \tag{29}$$

where Var is variance.

In the results of the reconstruction with added noise contamination (Table II) some interesting points can be raised. For enhancement one the value of the ratio k_1/k_2 plays an important role in the noise sensitivity. In our simulations when k_1/k_2 is 1.1 noise contamination in excess of 20 dB causes significant increases in degradation. However, below this level, the sensitivity to noise is similar to the conventional Born approximation. This threshold effect is because a_0 is given by (26) where it is clear that the smaller the difference $k_1 - k_2$ the greater will be the sensitivity to noise. It is found that if an error greater than 10% occurs in the estimation of a_0 then significant increases in degradation in the reconstruction occurs and for $k_1/k_2 = 1.1$ this occurs when the SNR > 20 dB. However, this threshold can be increased by increasing the ratio k_1/k_2. For enhancement two, noise sensitivity is also generally higher than that for the conventional Born approximation. The reason for this is that for enhancement two, the estimation of the additional coefficients a_{10} and a_{01} introduces additional uncertainty. However, this is offset by utilizing data from five different k thereby causing some reduction in noise sensitivity due to averaging.

B. Asymmetric Objects

To further demonstrate our enhancements, reconstruction of an asymmetrical object is provided in this section. For asymmetric objects, the coefficients a_{mn} are different for different $\hat{\mathbf{k}}$. The asymmetric object we trial consists of three eccentric cylinders. The radii of the cylinders which make up

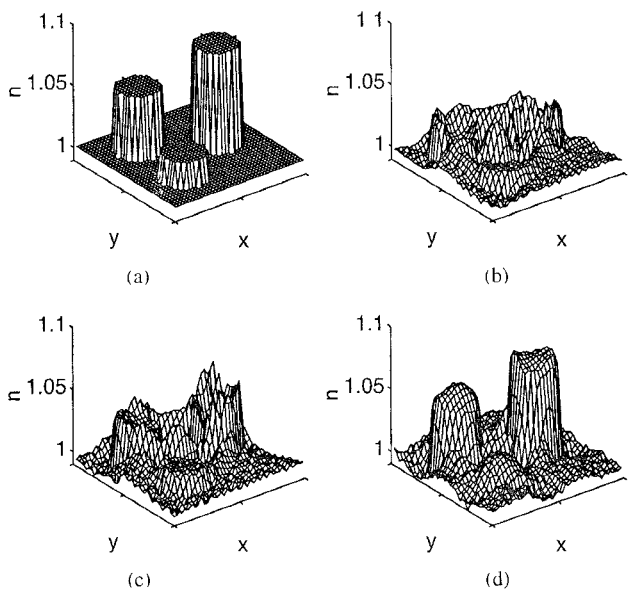

Fig. 9. Reconstruction of the asymmetric object defined in (30): (a) and (b) are, respectively, the original and conventional Born approximation; (c) and (d) are, respectively, reconstruction by invoking enhancement one and enhancement two.

the objects are all equal to 3λ. The exact configuration of the object is specified as

$$\begin{aligned} \text{Object:}\quad & n_1 = 1.02, \quad r_2 = 3\lambda, \quad \text{center} = (-4\lambda, -4.5\lambda) \\ & n_2 = 1.05, \quad r_1 = 3\lambda, \quad \text{center} = (-4\lambda, 4.5\lambda) \\ & n_3 = 1.08, \quad r_2 = 3\lambda, \quad \text{center} = (4.5\lambda, 0). \end{aligned} \tag{30}$$

The results of reconstructing this object are shown in Fig. 9. Both enhancement one and two perform better than the conventional Born approximation. It is found that enhancement two gives a good estimation of the height (refractive index) of the cylinders in all cases. However, the profile of the cylinders are distorted. Results from other asymmetrical objects of this type provide similar findings.

VI. Discussion

From our simulation results, it has been demonstrated that both enhancement one and two provide significant improvements in the reconstruction quality of the conventional Born and Rytov approximations. Some further questions remain to be answered concerning the range of the validity of these enhancements, how the enhancements relate to the Rytov approximation and what additional computational requirements do the enhancements require.

A. Approximation Validity

For the conventional Born approximation we know the range of validity to be approximately specified as $(n-1)L < b\lambda$ where $b \approx 0.1 - 0.5$ [4]. To deduce a similar validity condition for our enhancements we must consider the underlying approximations invoked. In our enhancements essentially two approximations have been invoked.

The first approximation utilized is that of the WKB approximation (16) as a representation of the total field. Such an approximation is predicated upon refraction predominating over reflection which requires that spatial variations of the refractive index n be small. To get an objective measure of this we may assume that the strength of the reflections must be smaller than the transmitted wave for the approximation to be valid corresponding to a reflection ratio of less than one half. If we assume that the discontinuities are along planar interfaces the reflection coefficient can be given as

$$\rho = \frac{n_1 - n_2}{n_1 + n_2} \tag{31}$$

where n_1 and n_2 are the refractive indices either side of the interface. By ensuring $\rho < 0.5$ in (31) gives us a validity condition on our approximation as $0.75 < n_1/n_2 < 1.5$. Results of investigating this validity condition have been confirmed by previous investigation which suggest that it is an upper bound for the validity of (16) in [21].

The second approximation is introduced in (17) and relates to how well the various terms in our approximation can model the distortion function. The validity of this approximation is likely to be dependent on the shape and distribution of the refractive index. For enhancement one, this is likely to be similar to the conventional Born approximation except that the additional constant phase term will increase validity by up to a factor of two such that $(n-1)L < 2b\lambda$. This is because the phase reference is at the center of the object rather than the edge as for the conventional Born approximation. This represents an increase of two for the validity of the conventional Born approximation. For enhancement two, however, the validity is even greater than this since the distortion function is likely to be well modeled if the wavefronts vary linearly with $\mathbf{x}$.

Conclusions of this nature are supported by the simulation results. Enhancement one is valid for a wider class of objects that the conventional Born approximation but breaks down when $(n-1)L > \lambda$ as in Fig. 7. Under enhancement two it can be observed that it performs well for all the circularly symmetric objects. However, when significant deviations from a simple refractive index distribution occur (as in Fig. 9), degradation in the reconstruction increases.

B. Relation to the Rytov Approximation

Although our enhancements have been obtained from consideration of the Born approximation, it is also worthwhile to consider why it outperforms the Rytov approximation and how it may relate to the Rytov approximation [4].

To understand why our enhancements perform better than the Rytov approximation, we need to consider the approximation in more detail. In some ways our enhancements can be likened to the Rytov approximation since we are devising a better approximation to E_z the total field by including a linear phase term. Although this linear phase term can be likened to the Rytov approximation which utilizes an arbitrary function to represent the phase the Rytov approximation neglects the term

$$\nabla \ln \left[\frac{E_z(\mathbf{x}, k)}{E_z^i(\mathbf{x}, k)}\right] \cdot \nabla \ln \left[\frac{E_z(\mathbf{x}, k)}{E_z^i(\mathbf{x}, k)}\right] \tag{32}$$

TABLE I
A COMPARISON OF THE COEFFICIENTS OBTAINED FROM THE SIMULATION RESULTS OF OUR ENHANCEMENTS TO THOSE FROM THE APPROXIMATE THEORY (20)

Numerical Example	Estimated Coefficients from (20)		Estimated coefficients from enhancement one	Estimated Coefficients from enhancement two	
	a_{00}	$\|(a_{10}, a_{01})^T\|$	a_{00}	a_{00}	$\|(a_{10}, a_{01})^T\|$
figure 4	0.942	0.050	0.784	0.834	0.052
figure 5	1.885	0.100	1.426	1.690	0.099
figure 6	1.414	0.031	0.968	1.437	0.036
figure 7	1.414	0.044	1.306	1.506	0 031
figure 8	0.930	0.028	0.885	1.049	0.026

TABLE II
SIMULATION RESULTS OF NMSE FOR WHEN NOISE CONTAMINATION WITH SNR OF 20 AND 25 dB ARE ADDED TO THE DATA. THE DEFINITIONS OF SNR AND NMSE ARE PROVIDED IN SECTION V-A

Numerical Example	Born Approximation		Enhancement One		Enhancement Two	
	20 dB	25 dB	20 dB	25 dB	20 dB	25 dB
figure 4	1.43	0.88	1.84	0.75	2.7	1.01
figure 5	1.97	1.35	5.8	2.49	5.2	2.1
figure 6	4.19	1.65	6.14	2.25	6.01	2.4
figure 7	1.73	0.99	14.0	4.15	7.8	3.4
figure 8	5.49	2.18	3.63	1.25	4.8	2.01

which causes the Rytov approximation to perform worse than the Born approximation for objects with large deviations in refractive index [4]. In our enhanced approximations, this term is not neglected and thus our enhanced approximation performs better for objects with larger deviations in refractive index than the Rytov approximation.

C. Computational Considerations

Our enhancements show that both enhancement one and two offer improvements over the Born and Rytov approximations. These improvements, however, must be weighed against the computational costs.

The additional computational cost for implementing enhancement one is low. This is because we only require additional computation for (26), which is a straightforward calculation.

The additional computation cost for enhancement two is higher, however, because we have to perform an optimization (27) over a total of five wavenumbers. This requires an increase in computational time by approximately a factor of 10–15 when measurements from five wavenumbers are used. However, the computational competitiveness of this method is still good in comparison to techniques based on exact descriptions of wave motion.

The other significant increase in load will be acquiring data from a range of frequencies. For enhancement one, this data is only required at one other frequency differing by approximately 10% from the first measurement. For enhancement two, however, measurements from five wavenumbers over a broadband are required. For measurement systems that use wideband pulses to probe the object, this may not be a problem since the wideband information in principle is readily available. However, for CW measurement systems additional scans of the object will be required at the different wavenumbers.

VII. CONCLUSION

An important contribution of the research presented here is the interpretation of the effects of refractive media on the Born approximation. In particular we demonstrate that it can

be likened to additional phase and translation of the observed object spectrum that is different for each angle of incidence $\hat{\mathbf{k}}$.

We further show how this phase and translation can be estimated from the measurement data to improve on the quality of the reconstruction. The concrete manifestation of this approach is an algorithm that is based on the techniques utilized in conventional diffraction tomography. The numerical results generated by this algorithm suggest that in general it can be expected to provide reconstructions that are more accurate than those generated by the conventional Born approximation. Considerations of the validity of the approximation for enhancement one indicate that it is an improvement over the Born approximation by a factor of two. For enhancement two, the range of validity is even larger than this. Moreover, we also show that the enhancements perform better than the Rytov approximation for objects with large deviations in refractive index.

We hope that through an approach of this kind improved reconstruction quality is achievable without the increased complexity of a full-wave description of the imaging or inverse scattering problem.

REFERENCES

[1] L. Jofre, M. S. Hawley, A. Broquetas, E. Reyes, M. Ferrando, and A. R. Elias-fuste, "Medical imaging with a microwave tomographic scanner," *IEEE Trans. Biomed. Eng.*, vol. 37, no. 3, pp. 303–312, Mar. 1990.

[2] J.-C. Bolomey, "Recent European developments in active microwave imaging for industrial, scientific, and medical applications," *IEEE Trans. Microwave Theory Tech.*, vol. 37, no. 12, pp. 2109–2117, Dec. 1989.

[3] J. E. Molyneux and A. Witten, "Diffraction tomographic imaging in a monostatic measurement environment," *IEEE Trans. Geosci. Remote Sensing*, vol. 31, no. 2, pp. 507–511, Mar. 1993.

[4] M. Slaney, A. C. Kak, and L. E. Larsen, "Limitations of imaging with first-order diffraction tomography," *IEEE Trans. Microwave Theory Tech.*, vol. MTT-32, no. 8, pp. 860–874, Aug. 1984.

[5] L. Garnero, A. Franchois, J.-P. Hugonin, C. Pichot, and N. Joachimowicz, "Microwave imaging-complex permittivity reconstruction by simulated annealing," *IEEE Trans. Microwave Theory Tech.*, vol. 39, no. 11, pp. 1801–1807, Nov. 1991.

[6] Z. Zhao and N. H. Farhat, "Tomographic microwave diversity image reconstruction employing unitary compression," *IEEE Trans. Microwave Theory Tech.*, vol. 40, no. 2, pp. 315–322, Feb. 1992.

[7] S. Caorsi, G. L. Gragnani, and M. Pastorino, "A multiview microwave imaging system for two-dimensional penetrable objects," *IEEE Trans. Microwave Theory Tech.*, vol. 39, no. 5, pp. 845–851, May 1991.

[8] K. I. Schultz and D. L. Jaggard, "Microwave projection imaging for refractive objects: A new method," *J. Opt. Soc. Am. A*, vol. 4, no. 4, pp. 1773–1782, 1987.

[9] W. C. Chew and Y. M. Wang, "Reconstruction of two-dimensional permittivity distribution using the distorted Born iterative method," *IEEE Trans. Med. Imag.*, vol. 9, pp. 218–225, 1990.

[10] R. H. T. Bates, V. A. Smith, and R. D. Murch, "Manageable multidimensional inverse scattering theory," *Phy. Rep.*, vol. 201, no. 4, pp. 185–277, Apr. 1991.

[11] R. D. Murch, D. G. H. Tan, and D. J. N. Wall, "Newton–Kantrovich method applied to two-dimensional inverse scattering for an exterior Helmholtz problem," *Inverse Problems*, vol. 4, no. 4, pp. 1117–1128, 1988.

[12] G. Beylkin, "Imaging of discontinuities in the inverse scattering problem by inversion of a causal generalized radon transform," *J. Math. Phys.*, vol. 26, no. 1, pp. 99–108, Jan. 1985.

[13] R. J. Wombell and R. D. Murch, "The reconstruction of dielectric objects from scattered field data using the distorted-wave born approximation," *J. Electromagn. Waves Applicat.*, vol. 7, no. 5, pp. 687–702, 1993.

[14] R. H. T. Bates, W. M. Boerner, and R. G. Dunlop, "An extended Rytov approximation and its significance for remote sensing and inverse scattering," *Optics Communications*, vol. 18, no. 4, pp. 421–423, Sept. 1976.

[15] M. Soumekh, "An improvement to the Rytov approximation in diffraction tomography," *IEEE Trans. Ultrason., Ferroelect., Freq. Contr.*, vol. UFFC-33, no. 4, pp. 394–401, July 1986.

[16] R. D. Murch, "An extended Born approximation," *Inverse Problems*, vol. 8, no. 4, pp. L5–L11, Aug. 1992.

[17] D. S. Jones, *Acoustic and Electromagnetic Waves*. Oxford: Oxford Univ. Press, 1986.

[18] R. N. Bracewell, *The Fourier Transform and its Applications*, 2nd ed. New York: McGraw-Hill, 1978.

[19] A. J. Devaney, "A filtered backpropagation algorithm for diffraction tomography," *Ultrasonic Imaging*, vol. 4, no. 4, pp. 336–350, Oct. 1982.

[20] K. J. Langenberg and H. Chaloupka, "Canonical two-dimensional inverse scattering problem," in *The ACES Collection of Canonical Problems Set 1*, H. A. Sabbagh, Ed. The Applied Computational Electromagnetics Society, 1990, pp. 100–102.

[21] R. D. Murch, "An evaluation of a Ray-tracing volume source formulation of scattering," *J. Acoust. Soc. Am.*, vol. 96, no. 3, pp. 1881–1886, Sept. 1994.

R. D. Murch (S'85–M'90) received the bachelor's and Ph.D. degrees in electrical and electronic engineering from the University of Canterbury, Christchurch, in 1986 and 1990, respectively. For the Ph.D., he investigated electromagnetic inverse scattering problems under the supervision of Prof. R. H. T. Bates (deceased 1990).

From 1990 to 1992, he was a Post Doctorate Fellow at the Department of Mathematics and Computer Science at Dundee University, Scotland. He joined the Hong Kong University of Science and Technology in May 1992, where he is now an Assistant Professor in the Department of Electrical and Electronic Engineering. His research interests include investigating new approaches to approximately calculating electromagnetic scattering from 3-D objects, inverse scattering, and propagation prediction/antenna design for wireless communications.

Dr. Murch is a Chartered Engineer and a member of IEE. In 1993, he won a URSI Young Scientist Award.

T. K. K. Chan was born in Hong Kong in 1967. He received his B.Sc. (Hons 1) in applied physics from Hong Kong Baptist College in 1991. In 1993, he completed his M.Phil. (with distinction) in electrical and electronic engineering from the Hong Kong University of Science and Technology, Kowloon, Hong Kong.

He is currently employed in the Hong Kong electronics industry and has research interests in the areas of imaging and robotics.

Mr. Chan was awarded the Wong Kwok Shuen Memorial Scholarship for academic merit in 1989.